On-axis diffractional behavior of two-dimensional pupils

Manuel Martínez-Corral, Pedro Andrés, and Jorge Ojeda-Castañeda

We show that, at any Fresnel number, a suitable one-dimensional Fourier transform relates the complex-amplitude distribution along the optical axis with the zero-order circular harmonic of the amplitude transmittance of a two-dimensional diffracting screen. First, our general result is applied to recognize that any rationally nonsymmetric screen generates an axial-irradiance distribution that exhibits focal shift. In this way we identify a wide set of two-dimensional screens that produce the same focal shift as that produced by the clear circular aperture. Second, we identify several apodizers for shaping the axial-amplitude distribution. We discuss some examples for achieving high-precision focusing, axial hyperresolution, or high focal depth.

Key words: Axial irradiance, focal shift, apodizers, Strehl ratio versus defocus.

1. Introduction

Imaging devices are commonly designed by use of geometrical optics, with the purpose of concentrating optical rays in certain prespecified areas. Thus one expects that an imaging device will concentrate energy, for instance, at certain positions along the optical axis. However, when using diffractive optics in optical interconnects or for evaluating the performance of diffracting screens as apodizers, one must describe the irradiance concentration capabilities in terms of physical optics.

Several authors have considered analysis of the axial impulse response of an optical system with a two-dimensional (2-D) pupil by using a convenient set of functions that describes as a series expansion the radial variations of the pupil. For example, Walsh functions,[1] Chebyshev polynomials,[2] and Zernike polynomials[3] have been used. Legendre polynomials have been employed for tailoring the axial impulse response with the purpose of achieving arbitrarily high focal depth[4] or for shaping the focal power spectrum of zone plates.[5] In previous years, efforts have been addressed to study the loss of symmetry of the axial impulse response that appears when optical systems of small Fresnel number[6–12] are used.

The aim of this paper is to report a compact analytical expression for evaluating the axial-amplitude distribution generated by a 2-D diffracting screen. The formulation holds for any rotationally nonsymmetric screen, with or without central obscuration, and for any Fresnel number. Our formula consists of two factors. As in McCutchen's theorem,[13] the first factor involves a suitable one-dimensional (1-D) Fourier transform of the zero-order circular harmonic of the amplitude transmittance of the diffracting screen. The second factor is $N - 2W_{20}$, where N is the Fresnel number of the pupil and W_{20} is the defocus coefficient, and it is responsible for the focal-shift effect shown by the axial-irradiance distribution. Our general result is illustrated here by evaluation of the focal shift produced by certain pupils without radial symmetry, and we propose some apodizers for shaping the axial irradiance. Other applications will be developed elsewhere.

In Section 2 we formulate the basic theory for evaluating the axial-amplitude distribution produced by an arbitrary generalized pupil, at any Fresnel number. In Section 3 we discuss the focal-shift effect produced by any pupil without radial symmetry. Finally, in Section 4 our formulation is applied to design certain apodizers for shaping the amplitude distribution along the optical axis.

2. Irradiance Distribution Along the Optical Axis

We start by considering a rather general set of 2-D diffracting screens that are characterized by having an amplitude transmittance equal to zero in both a

M. Martínez and J. Ojeda-Castañeda are with the Departamento de Optica, Universidad de Valencia, Burjassot 46100, Spain. P. Andrés is with the Departamento de Ciencias Experimentales, Universitat Jaume I, Castellón 12080, Spain. J. Ojeda-Castañeda's permanent address is Instituto Nacional de Astrofísica, Optica y Electrónica, Apartado Postal 216, Puebla 72000, Puebla, México.

Received 7 January 1993; revised manuscript received 23 August 1993.

0003-6935/94/112223-07$06.00/0.

central region and an external region. The transmittance is different from zero in an amorphic region that is confined to an annular area centered in the optical axis, as is shown in Fig. 1(a). The external radius of the pupil is a, and the internal radius is ϵa, where ϵ $(0 \leq \epsilon < 1)$ is the central obscuration ratio. Note that in the particular case of $\epsilon = 0$, the amplitude-transmittance function is confined into a circular area. Hence the complex-amplitude transmittance of any 2-D diffracting screen is hereafter mathematically expressed as an annular generalized pupil function, $p(r, \theta)$.

According to Ref. 12, if this screen is illuminated by a converging, monochromatic spherical wave, the Fresnel–Kirchhoff diffraction equation for the amplitude distribution along the optical axis is

$$u(z) = [-i/\lambda f(f+z)]\exp(ikz)\int_0^{2\pi}\int_{\epsilon a}^{a} p(r, \theta) \times \exp[-ikzr^2/2f(f+z)]r\,dr\,d\theta, \quad (1)$$

where λ is the wavelength of the incident light, $k = 2\pi/\lambda$, z denotes the axial coordinate as measured from the paraxial focal point, and f represents the focal length of the optical system, as is shown in Fig. 1(b).

Next, it is convenient to separate the angular variation from the radial contribution to the transmittance by expansion of the amplitude-transmittance function into its circular-harmonic series; that is,

$$p(r, \theta) = \sum_{m=-\infty}^{+\infty} p_m(r)\exp(im\theta), \quad (2)$$

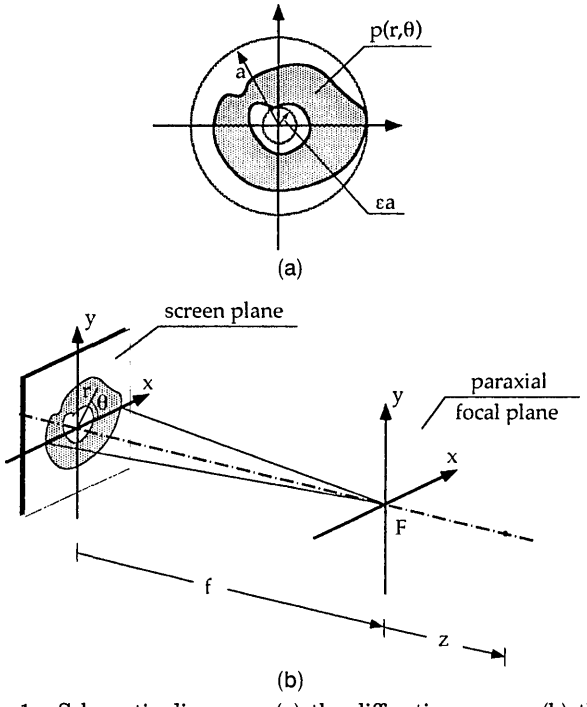

Fig. 1. Schematic diagram: (a) the diffracting screen, (b) the optical setup under consideration.

where

$$p_m(r) = (1/2\pi)\int_0^{2\pi} p(r, \theta)\exp(-im\theta)\,d\theta. \quad (3)$$

In Eq. (2), $p_m(r)$ is the radial component of the mth circular harmonic of $p(r, \theta)$. In other words, $p_m(r)$ is a function whose value, for every r, is the mth coefficient of the Fourier-series expansion of the aximuthal variation of the generalized pupil function.

Now, by substituting Eq. (2) into Eq. (1) and by performing the integration with respect to θ, we obtain

$$u(z) = [-ik/f(f+z)]\exp(ikz)\int_{\epsilon a}^{a} p_0(r) \times \exp\{-ik[a^2z/2f(f+z)](r/a)^2\}r\,dr, \quad (4)$$

where $p_0(r)$, the zero-order circular harmonic, represents for each r the azimuthal average of the generalized pupil function along a centered ring with radius r, as is shown graphically in Fig. 2.

Now, it is possible to convert Eq. (4) into a 1-D Fourier transform under a geometrical mapping that translates the annular interval $[\epsilon a, a]$ for every value of ϵ into the 1-D interval $[-1, 1]$. The geometrical transformation reads as

$$\zeta = 2\frac{(r/a)^2 - \epsilon^2}{1 - \epsilon^2} - 1, \qquad q_0(\zeta) = p_0(r). \quad (5)$$

In this way we have, except for an irrelevant phase factor, the complex-amplitude distribution along the optical axis:

$$u(z) = [\pi a^2(1-\epsilon^2)/2\lambda f(f+z)]\int_{-1}^{1} q_0(\zeta) \times \exp\{-i2\pi[a^2(1-\epsilon^2)z/4\lambda f(f+z)]\zeta\}\,d\zeta. \quad (6)$$

It is apparent from Eq. (6) that the complex-amplitude distribution along the optical axis is related with the 1-D Fourier transform of the mapped

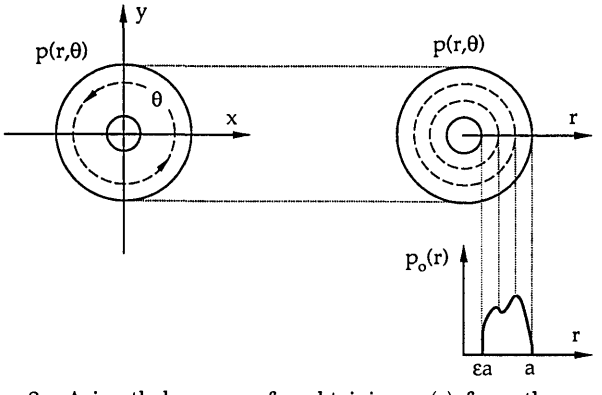

Fig. 2. Azimuthal average for obtaining $p_0(r)$ from the pupil function along any centered ring with radius r.

zero-order circular harmonic of the pupil function, $q_0(\zeta)$. Furthermore, Eq. (5) indicates that from a given mapped function, $q_0(\zeta)$, it is possible to generate a whole family of apodized pupils, $p_0(r)$; they have the same transmittance profile but different central obscuration ratios ϵ, as shown in Fig. 3. Consequently Eq. (6) shows that any pair of functions belonging to the same family has, aside from a scaling factor, the same on-axis diffractional behavior.

Moreover, Eq. (6) also permits us to state the following properties, which may be useful in metrology. Zero-axial irradiance is achieved if, and only if, the angular average of the generalized pupil is equal to zero.[14] Besides, since the axial-amplitude distribution is related to the 1-D Fourier transform of $q_0(\zeta)$, it appears that the amplitude at the paraxial focus, $z = 0$, is proportional to the mean value of $q_0(\zeta)$ or equivalently to the area of the function $p_0(r)$. Thus

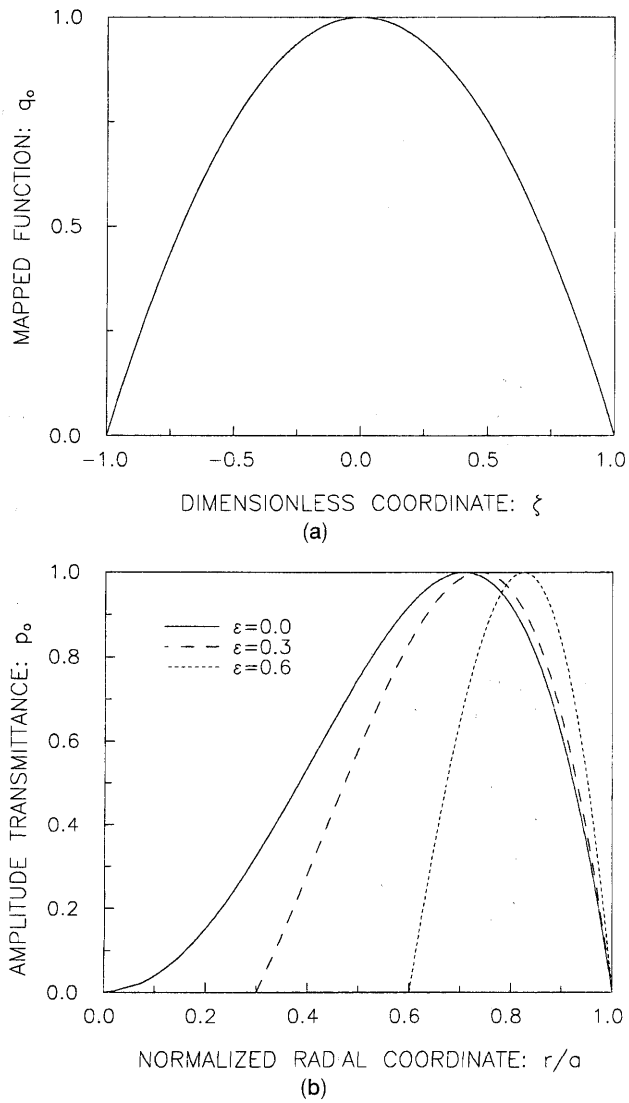

Fig. 3. Generation of a family of apodized pupils with the same transmittance profile but with different central obscuration ratios: (a) generating function $q_0(\zeta) = 1 - \zeta^2$, (b) some members of the family of 2-D annular pupils generated with the above $q_0(\zeta)$.

at the focus the axial irradiance is zero if, and only if, the mean value of the function $q_0(\zeta)$ is equal to zero. We take advantage of this fact in Section 4.

Finally, it is convenient to rewrite Eq. (6) in terms of the following definitions:

$$N = a^2(1 - \epsilon^2)/\lambda f, \quad W_{20} = Nz/2(f + z), \quad h(W_{20}) = u(z), \tag{7}$$

where N denotes the Fresnel number of the annular aperture, i.e., the number of Fresnel zones that cover the exit pupil from the geometrical focus, while W_{20} is the well-known defocus coefficient in the imaging formation formalism, which is proportional to the modified dimensionless Lommel variable $u_N = 2\pi Nz/(f + z)$, as defined by Li and Wolf in Ref. 6. These definitions are valid for any annular aperture, and they contain as a particular case the circular aperture, $\epsilon = 0$.

If we now substitute Eq. (7) into Eq. (6), we obtain

$$h(W_{20}) = [\pi(N - 2W_{20})/2f] \int_{-1}^{1} q_0(\zeta)\exp(-i\pi W_{20}\zeta)\mathrm{d}\zeta, \tag{8}$$

which is a generalization of the result of Ref. 12. In fact, the difference is that in Ref. 12 a circular pupil was considered, and here we consider any rotationally nonsymmetric pupil.

We emphasize that this analytical tool permits us to establish that the axial-irradiance distribution, $I(W_{20}) = |h(W_{20})|^2$, generated by any 2-D diffracting screen exhibits focal shift. Furthermore, the above result is also useful for designing apodizers for shaping the amplitude distribution along the optical axis. We next show both facts.

3. Focal Shift in Apodized Screens

If a monochromatic spherical wave is focused by a diffraction-limited optical system of sufficiently small Fresnel number, then the axial point of maximum irradiance does not coincide with the geometrical focus, but it is located closer to the aperture.[6] This nonsymmetrical behavior appears if certain factors preceding the integral in the Fresnel–Kirchhoff equation for scalar diffraction are preserved,[9] as was made in our formalism.

The factor $N - 2W_{20}$, with W_{20} as the functional variable, which precedes the diffraction integral in Eq. (8), is responsible for the loss of symmetry in the irradiance distribution along the optical axis for both radially symmetric and radially nonsymmetric annular generalized pupils. This effect is important when the value of the Fresnel number, N [see Eq. (7)], is sufficiently small.

In other words any pair of diffracting screens whose zero-order circular harmonic has both the same profile and the same Fresnel number generates an identical axial-irradiance distribution. Therefore it is possible in principle to find several screens that

generate the same axial irradiance, and consequently they show the same focal shift. In particular the same on-axis behavior is exhibited by the clear annular aperture and by all the radially nonsymmetric annular pupils that fulfil the condition

$$p_0(r) = k, \qquad \epsilon a \le r \le a, \tag{9}$$

and zero elsewhere, where k is a constant ($0 < |k| < 1$). The requirement in Eq. (9) is equivalent to $q_0(\zeta) = k$. In Fig. 4(a) we show an element of this wide set of 2-D functions that satisfies Eq. (9). The normalized axial-irradiance distribution of this type of screen is depicted for $N = 2.5$ in Fig. 4(b). As is usual, the normalization is such that $I(W_{20} = 0) = 1$. We note from Fig. 4(b) that the position of the maximum value of the axial irradiance does not coincide with the geometrical focus ($W_{20} = 0$) but is shifted toward the aperture ($W_{20} < 0$).

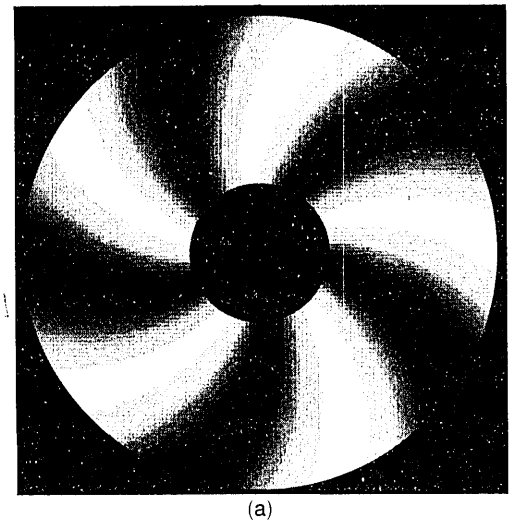

(a)

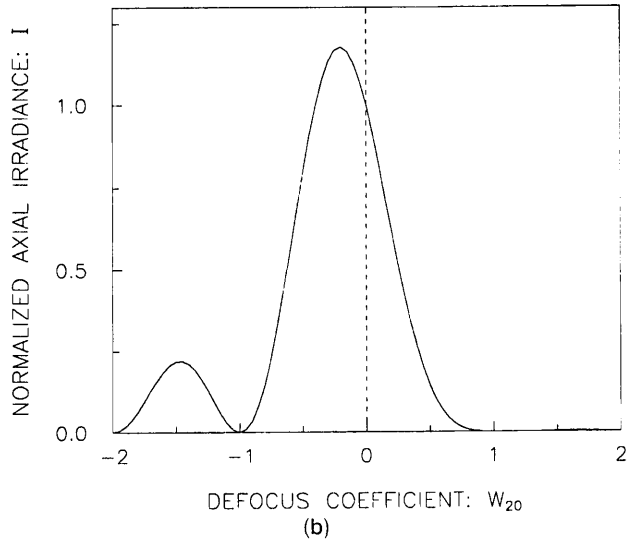

(b)

Fig. 4. Focal-shift effect produced by an absorbing screen whose azimuthally averaged amplitude transmittance is $p_0(r) = 0.5$: (a) gray-scale representation of the annular aperture, (b) normalized axial-irradiance distribution for $N = 2.5$. The normalized axial-irradiance distribution for the clear annular pupil is the same.

4. Apodizer Design

Inspection of Eq. (8) reveals that for a sufficiently high Fresnel number the axial-irradiance distribution generated by the 2-D screen $p(r, \theta)$ is proportional to the square of the 1-D Fourier transform of $q_0(\zeta)$. A result of this type is encountered in the standard analysis of imaging systems in which a Fourier transformation links the amplitude transmittance of a 1-D pupil filter with the amplitude distribution at the image plane.

This analogy can be exploited for designing apodizers that produce, along the optical axis, the same effect that a pupil filter would in an imaging formation context, as was pointed out in Ref. 15. In this way, if we have a 1-D pupil filter that decreases the outer lobes of the amplitude impulse response, which enlarges the central lobe, then we recognize that it is possible to obtain a whole family of 2-D screens for achieving high focal depth. Specifically, any member of the family of screens with $q_0(\zeta) = 1 - \zeta^2$ (see Fig. 3) is able to create high focal depth, as is shown in Fig. 5. The spreading of the central lobe increases the tolerance of the device to a defocus error.

Another possibility is to achieve the opposite effect, i.e., axial hyperresolution. In this case the profile of $q_0(\zeta)$ is the same as that of a 1-D hyperresolving filter, say, $q_0(\zeta) = \zeta^2$. In Fig. 6(a) we plot some elements, with different central obscuration ratios, of the family of apodized pupils that are mapped, with the transformation of Eq. (5), into the function $q_0(\zeta) = \zeta^2$. The normalized axial-irradiance distribution obtained with this type of apodizer is shown in Fig. 6(b). The outer lobes of the axial irradiance increase, but the central lobe narrows; in this way one is able to achieve an axially hyperresolving effect, which may be useful for precision focusing.[16]

The above results on apodizer design can be conveniently rephrased in mathematical terms for a wide range of generalized pupils. Let us assume that the

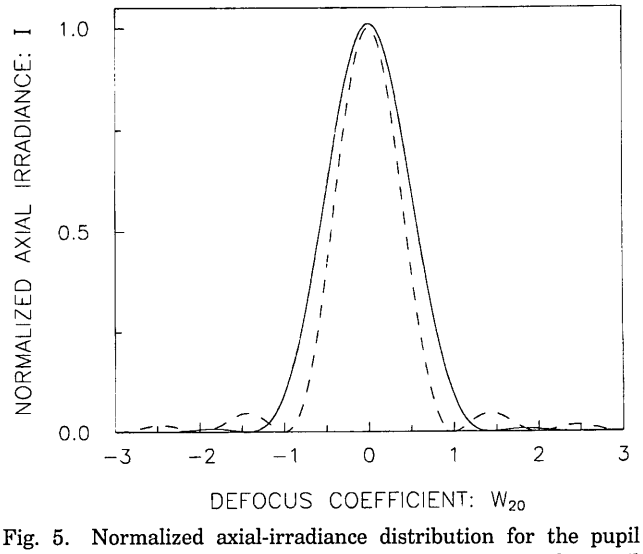

Fig. 5. Normalized axial-irradiance distribution for the pupil functions in Fig. 3(b) (solid curve) and for the clear annular pupil (dashed curve).

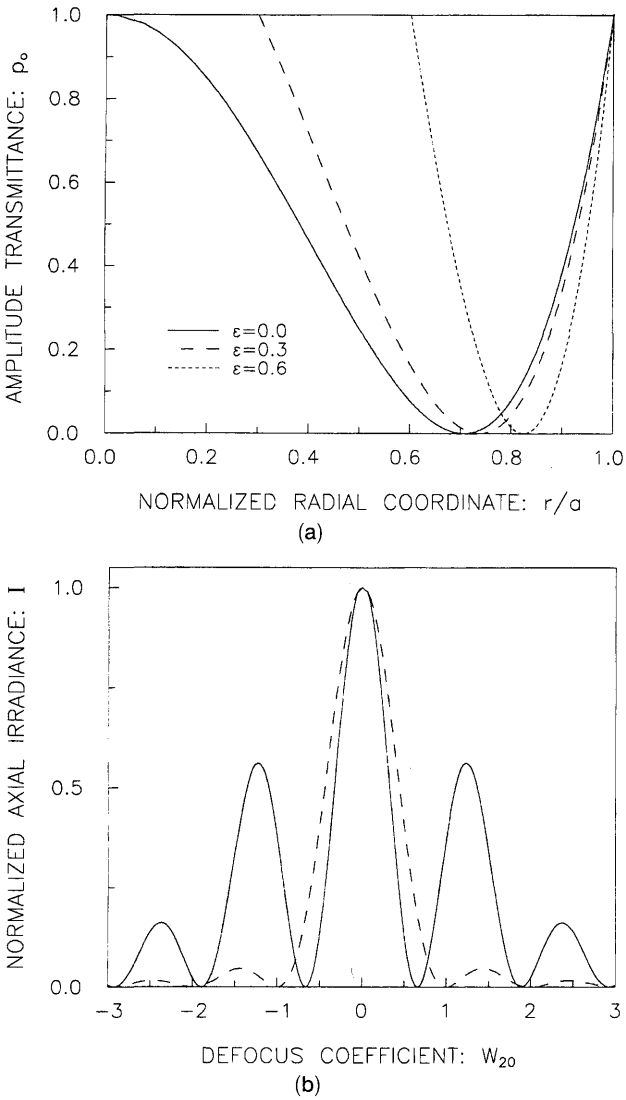

Fig. 6. Axial hyperresolving effect: (a) apodizers whose azimuthally averaged amplitude transmitance is mapped into the 1-D function $q_0(\zeta) = \zeta^2$, (b) normalized axial-irradiance distribution for these pupil functions (solid curve) and for the clear annular pupil (dashed curve).

mapped zero-order circular harmonic of the pupil function is expressible as a series of Legendre polynomials, $P_n(\zeta)$, that are a complete set of orthogonal functions for $-1 \le \zeta \le 1$; that is,

$$q_0(\zeta) = \sum_{n=0}^{+\infty} a_n P_n(\zeta). \tag{10}$$

Hence by substituting Eq. (10) into Eq. (8) and by taking into account that the Fourier transform of the n-order Legendre polynomial is proportional to the spherical Bessel function of the same order, j_n, we obtain, for a sufficiently high Fresnel number,

$$h(W_{20}) = (\pi N/f) \sum_{n=0}^{+\infty} (-i)^n a_n j_n(\pi W_{20}). \tag{11}$$

Therefore from Eq. (11) it is possible to evaluate the axial-irradiance distribution, $|h(W_{20})|^2$, of any annular generalized pupil function, with a variable central obscuration ratio, whose mapped zero-order circular harmonic is expressible as a series of Legendre polynomials. It is evident that the above-mentioned apodizers exemplify this case. Next, the present formulation is applied to propose two apodizers that may be useful for high-precision focusing.

It is interesting to note from Eq. (11) that at the paraxial focus, $W_{20} = 0$, the only contribution is due to the zero-order spherical Bessel function. Consequently if the amplitude transmittance profile of the apodizer in Eq. (10) excludes the Legendre polynomial of zero order, then the axial irradiance at the focus is zero, which may be useful for setting the focal point with high precision. As in Refs. 14 and 17, the present scheme uses a null rather than a maximum in the axial-irradiance distribution in order to locate the focus and to create a much greater (ideally, infinite) proportional change of a signal for a particular degree of defocusing.

The first apodizer, for achieving zero focal irradiance, is obtained by recognition that the first-order spherical Bessel function has the lowest spread among the nonzero-order functions of the same kind. Consequently our first proposed apodizer is represented by the function $q_0(\zeta) = P_1(\zeta) = \zeta$, whose associated 2-D representation is

$$p_0(r) = 2\,\frac{(r/a)^2 - \epsilon^2}{1 - \epsilon^2} - 1 \qquad \text{if } \epsilon a \le r \le a \tag{12}$$

and zero elsewhere, as is plotted in Fig. 7(a). Since in this case $a_n = \delta_{n,1}$ in Eq. (10), then according to Eq. (11), the axial-irradiance distribution is

$$|h(W_{20})|^2 = (\pi N/f)^2 [j_1(\pi W_{20})]^2. \tag{13}$$

The normalized irradiance distribution is plotted in Fig. 7(b). Here the normalization is such that the maximum value of the intensity is unity. It is convenient to observe that the zero value at the focal point is placed between two maxima, which are symmetrically located along the optical axis. These irradiance distribution properties can be exploited for setting a focusing technique with high precision.

However, care must be taken to avoid confusing any other zero value along the optical axis with the zero focal irradiance. This drawback can be eliminated if the zero focal value is created over a uniform background. Under this consideration we propose next a second apodizer for high-precision focusing.

For the second apodizer we suggest a pupil filter whose ideal axial-amplitude impulse response is

$$h(W_{20}) = 1 - \delta(W_{20}), \tag{14}$$

where δ denotes the Dirac delta function. For obtaining a realistic design one must consider that for the set of band-limited functions expressible as a series of spherical Bessel functions, Dirac's delta function

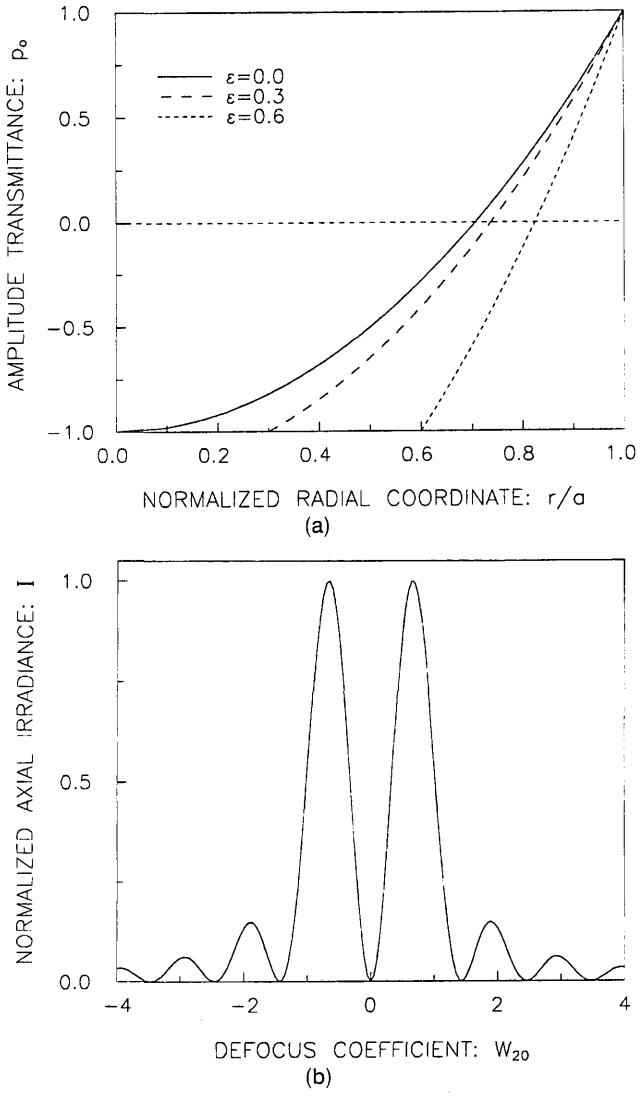

Fig. 7. First apodizer for high-precision focusing: (a) annular amplitude transmittance, (b) normalized axial-irradiance distribution.

$\delta(W_{20})$ is represented by $j_0(\pi W_{20}) = \sin(\pi W_{20})/(\pi W_{20})$. Hence the 1-D representation of the amplitude transmittance of our second apodizer is, regardless of a constant factor.

$$q_0(\zeta) = \delta(\zeta) - 0.5P_0(\zeta). \tag{15}$$

Now, it is well known that Dirac's delta function can be expressed in terms of a complete set of orthonormal function $\phi_n(\zeta)$ as

$$\delta(\zeta) = \sum_{n=-\infty}^{+\infty} \phi_n^*(0)\phi_n(\zeta). \tag{16}$$

If we particularize this relationship to the Legendre polynomials, we obtain

$$\delta(\zeta) = \sum_{n=0}^{+\infty} \frac{2n+1}{2} P_n(0)P_n(\zeta) \tag{17}$$

or equivalently

$$\delta(\zeta) = \lim_{M\to\infty} \sum_{m=0}^{M} [(-1)^m(2m)!(4m+1)/2^{2m+1}(m!)^2]P_{2m}(\zeta). \tag{18}$$

By substituting Eq. (18) into Eq. (15), we obtain

$$q_0(\zeta) = \lim_{M\to\infty} \sum_{m=1}^{M} [(-1)^m(2m)!(4m+1)/2^{2m+1}(m!)^2]P_{2m}(\zeta), \tag{19}$$

which describes an apodizer that approaches the realistic design in Eq. (15). The above complex-amplitude transmittance produces an arbitrarily wide axial-irradiance response. The 2-D amplitude-transmittance function associated with Eq. (19) is shown in Fig. 8(a) for several values of M and $\epsilon = 0$. Its

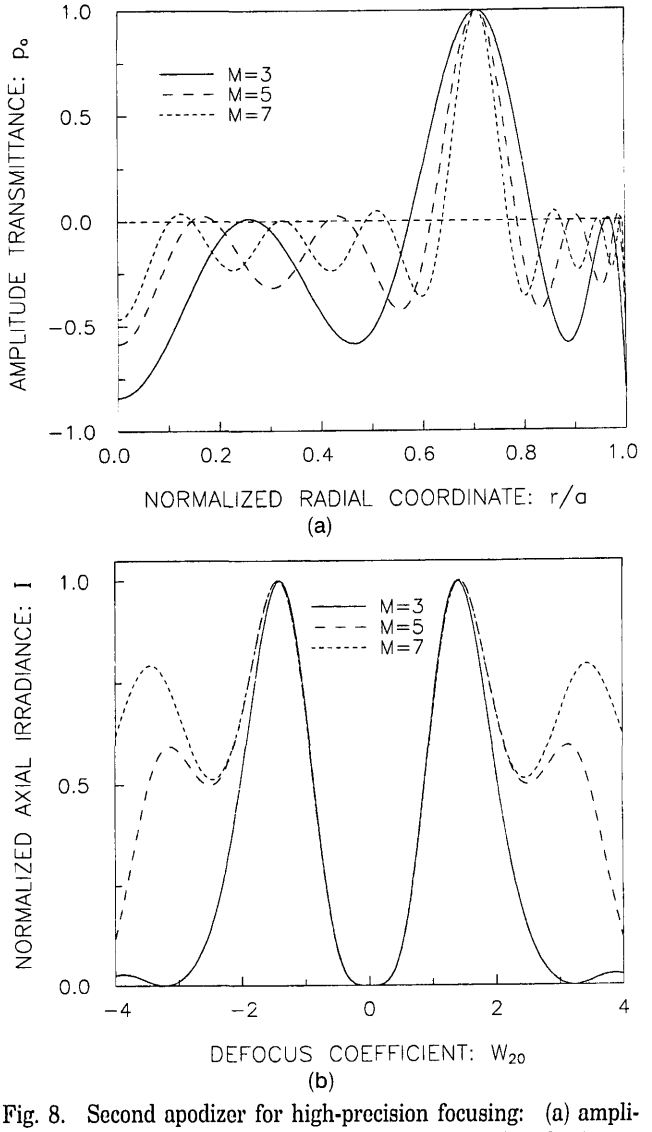

Fig. 8. Second apodizer for high-precision focusing: (a) amplitude transmittance, (b) normalized axial-irradiance distribution.

associated axial-amplitude response is

$$h(W_{20}) = \lim_{M\to\infty} \sum_{m=1}^{M} [(2m)!(4m+1)/2^{2m+1}(m!)^2] j_{2m}(\pi W_{20}), \tag{20a}$$

which can also be written as

$$h(W_{20}) = 1 - [\sin(\pi W_{20})/\pi W_{20}]. \tag{20b}$$

The square modulus of the sum in Eq. (20a) describes the axial irradiance, which is plotted in Fig. 8(b) for various values of M. From Fig. 8(b) we claim that our proposed apodizer is able to create zero axial irradiance along a narrow interval centered around the paraxial focus, over a background that approaches arbitrarily to uniformity. This result may be useful for setting a scheme for highly precise focusing.

5. Conclusions

We present a simple formula for evaluating in terms of the defocus coefficient W_{20} the on-axis diffractional behavior of any 2-D screen with arbitrary Fresnel number N. Specifically we show that the axial-amplitude distribution is proportional to the product of two factors. The first factor involves a 1-D Fourier transform of a suitably mapped version of the azimuthally averaged amplitude transmittance of the diffracting screen; the spatial frequency of the Fourier integral is proportional to the coefficient W_{20}. The second factor depends on both W_{20} and N but is independent of the amplitude transmittance of the screen.

Therefore we recognize that a diffracting screen, whose mapped transmittance function has the same profile as any 1-D pupil filter designed for apodizing the amplitude impulse response of an imaging system, produces, for N sufficiently high, an identical shaping in the axial-amplitude distribution. We illustrate our approach by designing some apodizers for achieving high-precision focusing, axial hyperresolution, or high focal depth. Our formula permits us to synthesize the apodizing function by using Legendre polynomials of any order.

Furthermore, we indicate that the second factor causes the loss of symmetry of the axial impulse response, which is appreciable when N is small. Consequently the same focal shift exhibited by the clear circular aperture is also exhibited by any screen whose amplitude transmittance averaged over any axially symmetric ring is constant.

This research was supported by an agreement between the Universitat Jaume I and the Fundació Caixa Castelló (grant CE.25.017/92), Spain. J. Ojeda-Castañeda and M. Martínez-Corral thank, respectively, the Dirección General de Investigación Científica y Técnica (Ministerio de Educación Ciencia, Spain), and the Consellería de Cultura, Educación Ciencia (Generalitat Valenciana, Spain) for financial support.

References

1. M. De and L. N. Hazra, "Walsh functions in problems of optical imagery," Opt. Acta **24,** 221–234 (1977).
2. M. Plight, "The rapid calculation of the optical transfer function for on-axis systems using the orthogonal properties of the Chebyshev polynomials," Opt. Acta **25,** 849–860 (1978).
3. V. N. Mahajan, "Zernike polynomials for imaging systems with annular pupils," J. Opt. Soc. Am. **71,** 75–85 (1981).
4. J. Ojeda-Castañeda and L. R. Berriel-Valdós, "Arbitrarily high focal depth with finite apertures," Opt. Lett. **13,** 183–185 (1988).
5. J. Ojeda-Castañeda, P. Andrés, and M. Martínez-Corral, "Zone plates with cells apodized by Legendre profiles," Appl. Opt. **29,** 1299–1303 (1990).
6. Y. Li and E. Wolf, "Focal shifts in diffracted converging spherical waves," Opt. Commun. **39,** 211–215 (1981).
7. J. H. Erkkila and M. E. Rogers, "Diffracted fields in the focal volume of a converging wave," J. Opt. Soc. Am. **71,** 904–905 (1981).
8. J. J. Stamnes and B. Spjelkavik, "Focusing at small angular apertures in the Debye–Kirchhoff approximation," Opt. Commun. **40,** 81–85 (1981).
9. M. P. Givens, "Focal shifts in diffracted converging spherical waves," Opt. Commun. **41,** 145–148 (1982).
10. V. N. Mahajan, "Axial irradiance and optimum focusing of laser beams," Appl. Opt. **22,** 3042–3053 (1983).
11. Y. Li, "Focusing nontruncated elliptical Gaussian beams," Opt. Commun. **68,** 317–323 (1988).
12. Y. Li and E. Wolf, "Focal shift in focused truncated Gaussian beams," Opt. Commun. **42,** 151–156 (1982).
13. C. W. McCutchen, "Generalized aperture and the three-dimensional diffraction image," J. Opt. Soc. Am. **54,** 240–244 (1964).
14. J. Ojeda-Castañeda, P. Andrés, and M. Martínez-Corral, "Zero axial irradiance by annular screens with angular variation," Appl. Opt. **31,** 4600–4602 (1992).
15. J. Ojeda-Castañeda, L. R. Berriel-Valdós, and E. Montes, "Bessel annular apodizers: imaging characteristics," Appl. Opt. **26,** 2770–2772 (1987).
16. B. R. Frieden, "On arbitrarily perfect imagery with a finite aperture," Opt. Acta **16,** 795–807 (1969).
17. J. Ojeda-Castañeda and G. Ramírez, "Zone plates for zero-axial irradiance," Opt. Lett. **18,** 87–89 (1993).